

FLICKER AS A TOOL FOR CHARACTERIZING PLANETS THROUGH ASTERODENSITY PROFILING

D. M. Kipping^{1,2}, F. A. Bastien³, K. G. Stassun^{3,4},
 W. J. Chaplin^{5,6}, D. Huber^{7,8}, L. A. Buchhave⁹

Draft version March 24, 2014

ABSTRACT

Variability in the time series brightness of a star on a timescale of 8 hours, known as “flicker”, has been previously demonstrated to serve as a proxy for the surface gravity of a star by Bastien et al. (2013). Although surface gravity is crucial for stellar classification, it is the mean stellar density which is most useful when studying transiting exoplanets, due to its direct impact on the transit light curve shape. Indeed, an accurate and independent measure of the stellar density can be leveraged to infer subtle properties of a transiting system, such as the companion’s orbital eccentricity via asterodensity profiling. We here calibrate flicker to the mean stellar density of 439 *Kepler* targets with asteroseismology, allowing us to derive a new empirical relation given by $\log_{10}(\rho_{\star} [\text{kg m}^{-3}]) = 5.413 - 1.850 \log_{10}(F_8 [\text{ppm}])$. The calibration is valid for stars with $4500 < T_{\text{eff}} < 6500 \text{ K}$, $K_P < 14$ and flicker estimates corresponding to stars with $3.25 < \log g_{\star} < 4.43$. Our relation has a model error in the stellar density of 31.7% and so has ~ 8 times lower precision than that from asteroseismology but is applicable to a sample ~ 40 times greater. Flicker therefore provides an empirical method to enable asterodensity profiling on hundreds of planetary candidates from present and future missions.

Subject headings: stars: activity — stars: solar-type — techniques: photometric — planetary systems

1. INTRODUCTION

In recent years, there has been an increased interest in exploiting time series brightness variations of stars to infer fundamental stellar properties. This upsurge has been largely motivated by the transiting exoplanet survey missions, such as CoRoT (Baglin et al. 2006) and *Kepler* (Borucki et al. 2009), which have provided an avalanche of high signal-to-noise and high cadence photometry. In addition, such missions require accurate stellar characterization to infer the correct parameters for the associated transiting planet candidates.

The strongest constraints on a star’s fundamental parameters using time series photometry come from asteroseismology (Chaplin & Miglio 2013), the study of stellar oscillations. Giants, sub-giants and bright dwarfs provide data on solar-like oscillations, and in these cases fundamental parameters may be determined to the percent level. Another technique, known as gyrochronology, exploits a star’s gradual angular momentum loss to date stars to $\sim 15\%$ accuracy using empirical calibrations from open clusters (Skumanich 1972; Barnes 2007; Epstein & Pinsonneault 2014). Here, the primary input is a stellar rotation period, which is revealed via rotational modulations in a photometric time series

(Walkowicz & Basri 2013). Recently, a new characterization technique has been proposed by Bastien et al. (2013) (B13), which uses the variability over an 8-hour timescale, “flicker”, as a proxy for the surface gravity of a star, g_{\star} . Flicker is able to reproduce $\log g_{\star}$ to within ~ 0.10 dex for FGK dwarfs and giants down to apparent magnitudes of 14 and is thought to be physically caused by stellar granulation on the star’s surface (Mathur et al. 2011; Cranmer et al. 2014). Whilst asteroseismology undoubtedly provides tighter constraints on a star’s basic parameters, the ability of flicker to infer $\log g_{\star}$ for a much larger number of stars in a magnitude-limited survey, such as *Kepler*, makes it highly appealing.

In conjunction with these recent developments in stellar characterization, several authors have recently explored how an accurate determination of the mean stellar density, ρ_{\star} , plus a high quality transit light curve may be used to infer various properties of an exoplanet (Kipping et al. 2012; Dawson & Johnson 2012; Kipping 2014). Asterodensity profiling (AP) compares the stellar density derived from the transit light curve shape (Seager & Mallen-Orn  las 2003), $\rho_{\star, \text{obs}}$, to some independent measure, $\rho_{\star, \text{true}}$. Relative differences can be caused by numerous phenomena, including orbital eccentricity and blend scenarios (Kipping 2014). Whilst asteroseismology directly yields the mean stellar density for those targets with detected oscillations (Ulrich 1986), flicker is currently only calibrated to surface gravity.

In this letter, we show that flicker is also able to determine the bulk density of a star to within $\sim 30\%$ across a wide range of spectral types and apparent magnitudes. This new empirical relation opens the door to conducting AP on many hundreds of transiting planet candidates detected by both *Kepler* and future missions. We describe our methodology for deriving this relation in §2, followed by an exploration of the results in §3. We close in §4 by discussing the potential of this relation for AP with both previous and future missions.

¹ Harvard-Smithsonian Center for Astrophysics, Cambridge, MA 02138; email: dkipping@cfa.harvard.edu

² NASA Carl Sagan Fellow

³ Dept. of Physics & Astronomy, Vanderbilt University, 1807 Station B, Nashville, TN 37235

⁴ Physics Dept., Fisk University, 1000 17th Ave. N, Nashville, TN 37208

⁵ School of Physics & Astronomy, University of Birmingham, Birmingham B15 2TT, UK

⁶ Stellar Astrophysics Centre, Aarhus University, Ny Munkegade 120, DK-8000 Aarhus C, Denmark

⁷ NASA Ames Research Center, Moffett Field, CA 94035

⁸ SETI Inst., 189 Bernardo Av., Mountain View, CA 94043

⁹ Centre for Star and Planet Formation, University of Copenhagen, DK-1350, Copenhagen, Denmark

2. METHODS

2.1. Seismic Data

In order to investigate whether a relation exists between flicker and mean stellar density, we first require an accurate catalog of stellar densities. Following B13, we identify the sample of *Kepler* targets for which asteroseismology oscillation modes have been detected as our “gold standard” catalog. These asteroseismology detections provide two immediate basic parameters: the average large frequency separation between consecutive overtones of the same spherical angular degree, $\Delta\nu$, and the frequency of maximum oscillations power, ν_{\max} . This latter term has been shown to be functionally dependent, to a good approximation, upon the surface gravity of the host star, g_* , and the effective temperature, T_{eff} , (Brown et al. 1991; Kjeldsen & Bedding 1995; Chaplin et al. 2008; Belkacem et al. 2011) via:

$$(\nu_{\max}/\nu_{\max,\odot}) \simeq (g_*/g_\odot)(T_{\text{eff}}/T_{\text{eff},\odot})^{-1/2}, \quad (1)$$

where $\nu_{\max,\odot}$ is Sun’s frequency of maximum oscillations power, $T_{\text{eff},\odot}$ is the Sun’s effective temperature and g_\odot is the Sun’s surface gravity. The derived surface gravity is therefore moderately dependent upon some independent measure of the effective temperature. The other basic seismic observable, $\Delta\nu$, scales with the star’s mean stellar density (Ulrich 1986) as:

$$(\Delta\nu/\Delta\nu_\odot) \simeq \sqrt{\rho_*/\rho_\odot}, \quad (2)$$

where ρ_\odot is the Sun’s mean density. In practice, this scaling is only approximate, and comparisons to individual model frequencies have shown temperature-dependent offsets of up to 2% in $\Delta\nu$ (White et al. 2011). Nevertheless, ρ_* has a weaker functional dependence on the input effective temperature than g_* and detailed seismic modeling allows for a refined measurement of ρ_* at the percent level. For this reason, we consider that the seismic densities are the most accurate and precise parameter revealed by asteroseismology and so provide an ideal catalog for later calibration to flicker estimates.

In this work, we use the catalogs of Huber et al. (2013) and Chaplin et al. (2014), which include 588 distinct *Kepler* target stars. In the case of the catalog from Chaplin et al. (2014), three different estimates of ρ_* are available, which vary very slightly due to different assumed effective temperatures and metallicities (Tables 4, 5 & 6). Of these, we preferentially employ Table 6 values wherever available (using high resolution spectroscopic stellar inputs from Bruntt et al. 2012), then Table 5 values (IRFM T_{eff} and field-average metallicity values) and finally Table 4 in all other cases (using SDSS-calibrated T_{eff} and field-average metallicity values). In the few cases where both Huber et al. (2013) and Chaplin et al. (2014) have independent measures, we use Huber et al. (2013) due to their use of dedicated spectroscopic inputs. In all cases, ρ_* uncertainties are also available, to provide the relevant weightings in the later regressions (see §2.3).

2.2. Flicker Data

Following Basri et al. (2011), and further described in B13, we measure the high-frequency stellar noise (F_8)

in the standard pipeline processed PDC-MAP (data release 21) *Kepler* long-cadence (30 min) light curves by calculating the root-mean-square (RMS) of the difference between the light curve and a box-car smoothed version of itself. Basri et al. (2011) originally defined the high-frequency noise using a 4-point smoothing, however B13 found that a 16-point (8-hr) smoothing yielded the cleanest correlation between the resultant F_8 and asteroseismically measured $\log g_*$. Large excursions in the light curve, caused, for example, by stellar flares, can artificially inflate the measured F_8 , resulting in erroneously low F_8 -based $\log g_*$. As such, we clip all 2.5σ or greater outliers in the light curve prior to taking the RMS. For stars with known transiting exoplanets, such as those in Huber et al. (2013), we additionally excise in-transit data points using the planetary orbital parameters publicly available through the NASA Exoplanet Archive (Akeson et al. 2013). We then correct this derived F_8 for shot noise contributions as described in B13. We compute F_8 for all available quarters of *Kepler* data and adopt our final estimate and associated uncertainty as the mean and standard deviation of the results, respectively.

2.3. Deming Regression

We here describe how we compute the “best-fitting” model describing the dependent variable, ρ_* , with respect to the independent variable, F_8 . We begin by noting that the correlation between these terms is close to linear using log-log scaling (see Fig. 1), similar to the case when B13 compared $\log g_*$ to F_8 . Switching to log-log scaling requires an adjustment of the uncertainties in both variables. Uncertainties are known for both the ρ_* (see §2.1) and F_8 (see §2.2) measurements, which may be converted into \log_{10} space using the general rule:

$$\sigma_{\log_{10} z} = (\sigma_z/z)/\log_e 10, \quad (3)$$

where z is each variable and σ_z is the associated uncertainty. Next, we consider that any model employed will itself be somewhat erroneous; i.e. there are not only uncertainties on the observables, but also in the model itself. For example, this could be because other terms not considered here also impact the observed flicker. We adopt a simple method to treat the model uncertainty by introducing a quadrature error term in the dependent variable, $\log_{10} \rho_*$, given by σ_{model} . This is similar to the way in which stellar “jitter” is often treated in radial velocity regressions (Wright 2005) and implicitly assumes that the model error does not vary with respect to the independent variable.

Although the fractional uncertainties on the $\log_{10} F_8$ measurements are typically much greater than those of $\log_{10} \rho_*$, we seek a regression technique which accounts for the appropriate weighting in both observables. Accordingly, our regression is performed in the least-squares framework, but specifically using the generalized Deming (1943) method, which accounts for the uncertainties in both variables. We adopt a simple linear slope model given by Equation 4, motivated by the visual correlation (see Fig. 1) and the simplicity of this model makes it attractive for wider use in the community.

$$\log_{10}(\rho_* [\text{kg m}^{-3}]) = \alpha + \beta \log_{10}(F_8 [\text{ppm}]). \quad (4)$$

To perform a Deming regression, we must determine the co-ordinates of the point along the model curve, $y(x)$ (where y and x denote the dependent and independent variables respectively), which has the closest Euclidean distance to each trial point, $\{x_i, y_i\}^T$. This is achieved by minimizing the metric $(x_{c,i} - x_i)^2 + (y(x_{c,i}) - y_i)^2$ with respect to $x_{c,i}$, where $\{x_{c,i}, y_{c,i}\}^T$ is the point along the curve $y(x)$ closest to the trial point $\{x_i, y_i\}^T$, which for our linear slope model gives:

$$x_{c,i} = (\alpha\beta + x_i + \beta y_i)(1 + \beta^2)^{-1}, \quad (5)$$

$$y_{c,i} = (\alpha + \beta(x_i + \beta y_i))(1 + \beta^2)^{-1}. \quad (6)$$

The least-squares merit function, which we numerically minimize with respect to α and β , is simply the weighted Euclidean distance between the observations and the model:

$$\sum_{i=1}^N \frac{(x_i - x_{c,i})^2 + (y_i - y_{c,i})^2}{\sigma_{x,i}^2 + \sigma_{y,i}^2}, \quad (7)$$

where in our specific case we have $x_i \rightarrow \log_{10}(F_8 [\text{ppm}])$, $y_i \rightarrow \log_{10}(\rho_* [\text{kg m}^{-3}])$, $\sigma_{x,i}^2 \rightarrow \sigma_{\log_{10}(F_8 [\text{ppm}])}^2$ and $\sigma_{y,i}^2 \rightarrow \sigma_{(\rho_* [\text{kg m}^{-3}])}^2 + \sigma_{\text{model}}^2$.

If we assume that the residuals of the dependent variable to the best-fitting model are approximately normally distributed, then one would expect, for a well-chosen σ_{model} , that the residuals divided by the respective uncertainties would be well described by the standard normal distribution. This can be checked by a subsequent least-squares regression of a normal distribution of zero mean but freely fitted variance to the distribution of the residuals. In practice, this is performed on the cumulative distribution of the residuals, rather than a probability density histogram, to avoid the choice of the bin-size affecting the results (Kipping 2013). In general, an arbitrary guess of σ_{model} will lead to a non-unity variance for this regressed normal distribution, but we iterate σ_{model} until this condition is satisfied in order to solve for the best σ_{model} .

3. RESULTS

3.1. Best-fitting Model

Following the method described in §2.3, the best-fitting (mean maximum likelihood) model is shown in Fig. 1. Our simple linear model provides an excellent description of the apparent correlation and the associated parameters are available in Table 1. To compute this model, we enforced several criteria to exclude some of the less reliable data.

- $1.2 < \log_{10}(F_8 [\text{ppm}]) \leq 2.2$ since we have relatively few points outside of this range.
- $\text{Range} \leq 1000 \text{ ppm}$ (defined in B13), since B13 find these points to be more frequently outliers.
- $4500 \leq T_{\text{eff}} < 6500 \text{ K}$ to avoid the very cool or hot stars in our sample.

TABLE 1

Best-fitting parameters between our linear model and the ρ_* - F_8 data for two sample choices.

	α	β	σ_{model}	Frac. Err. in ρ_*
“Good” sample	5.413	−1.850	0.138	31.7%
“Full” sample	5.471	−1.884	0.151	34.7%

- $K_P < 14$ since correcting F_8 for *Kepler* apparent magnitude is only calibrated up to this level (B13).

Note that the first criterion is equivalent to $3.25 \lesssim \log g_* \lesssim 4.43$ using the B13 relation, thus eliminating M & K dwarfs with insufficient photometric variability. These filters reduce the number of data points from 588 to 439. The 439 “good” points are denoted by circles in Fig. 1 and the ignored “bad” points are denoted by squares. Using only the good points, we find the model error is 0.14 dex (32% in ρ_*). Including all the data increases this to 0.15 dex (35% in ρ_*) and the fitted parameters are provided in Table 1.

Fig. 2 reveals that the residuals of the “good” sample appear approximately normally distributed. This means that if one knows the flicker of a star, one may construct an informative prior on $\log \rho_*$ using a normal distribution and the parameters provided in Table 1. For the Sun’s observed flicker (B13), our relation yields $\rho_* = (1.18 \pm 0.37) \rho_{\odot}$, compatible with the truth.

3.2. Comparison to the Surface Gravity Relation

We repeated our regression on the “good” sample replacing $\log_{10}(\rho_* [\text{kg m}^{-3}])$ with $\log_{10}(g_* [\text{cm s}^{-2}])$. Since the dependent variables have been changed and use different units, a fair comparison of their relative performance cannot be conducted by inspection of the residuals in the dependent variables. Instead, we invert the best-fitting model to predict F_8 as a function of the dependent variable and then compute the residuals in the F_8 measurements between the two models.

We find that the ρ_* model has a standard deviation in $\log_{10}(F_8 [\text{ppm}])$ of 0.0866 dex, versus 0.0824 dex for the $\log g_*$ model. We also note that the Pearson’s correlation coefficient is -0.927 for the ρ_* model but -0.934 for the $\log g_*$ model. We therefore conclude that surface gravity is a slightly better dependent variable to correlate against F_8 , although clearly ρ_* does an excellent job too (see Fig. 1). This weakly supports the hypothesis that flicker is most directly tracing surface features such as granulation (Cranmer et al. 2014), rather than internal processes. Further support of this is found when we compare M_*/R_* to F_8 , causing the correlation coefficient to drop to -0.928 . The ρ_* relation is likely a good match simply due to the expected evolutionary correlation between M_*/R_*^2 and M_*/R_*^3 . Nevertheless, the ρ_* relation is more useful when analyzing exoplanet transits, since this term directly affects the light curve shape (Seager & Mallen-Orn  las 2003).

4. DISCUSSION

4.1. Flicker as an Input for Asterodensity Profiling

Asterodensity profiling (AP) has recently emerged as a valuable tool for characterizing exoplanets using time series photometry (Kipping et al. 2012; Sliski & Kipping 2014; Kipping 2014). AP exploits the fact that for a

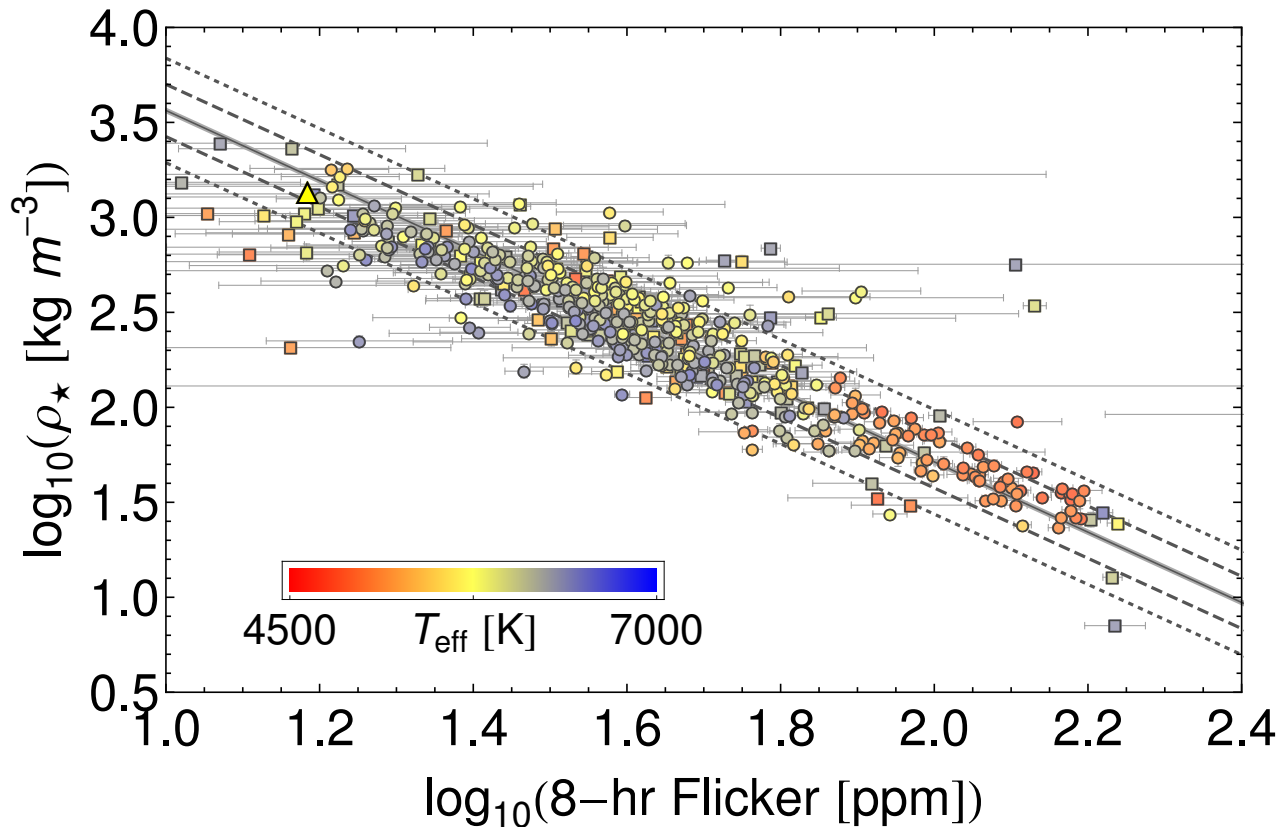


FIG. 1.— Empirical relationship between stellar density, ρ_* , and the 8-hour flicker, F_8 . Squares are unreliable points not used in regressing the best-fitting linear relation (solid line). Dashed and dotted lines show the 1σ and 2σ confidence regions. Points are color coded by the effective temperature and the Sun is marked with a triangle.

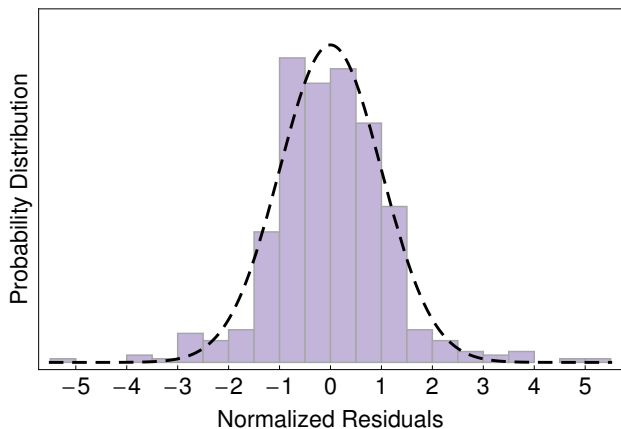


FIG. 2.— Distribution of the residuals of $\log_{10}(\rho_* [\text{kg m}^{-3}])$ to best-fitting linear model for the “good” sample, where we have normalized each residual by the associated uncertainty. The black dashed line is a standard normal distribution.

planet on a Keplerian circular orbit transiting an unblended star with a symmetric intensity profile, the shape of the light curve reveals $\rho_{*,\text{obs}}$ (Seager & Mallen-Orn  las 2003). If any of the idealized assumptions are invalid, then $\rho_{*,\text{obs}}$ will differ from the true value, $\rho_{*,\text{true}}$, and the direction and magnitude of the discrepancy reveals information about the transiting system (Kipping 2014). Using independent ρ_* estimates from asteroseismology, Sliski & Kipping (2014) provide an example of the utility

of AP by showing that the false positive rate of transiting planet candidates associated with giant stars is much higher than that of dwarf stars.

In this work, we have shown that flicker may also be used as an input for the independent measure of $\rho_{*,\text{true}}$ required for AP. Despite uncertainties in ρ_* increasing to $\sim 30\%$ from a flicker-based determination versus $\sim 4\%$ using asteroseismology, flicker can be used on many more targets in a magnitude-limited photometric survey like *Kepler*, since it works reliably down to $K_P = 14$ (see later discussion in §4.2). We do not claim that the derived relation is the optimal choice of regressors or parametric form, merely that it provides a simple, empirical recipe for estimating ρ_* . For example, including effective temperature may improve the relation, since cooler stars seem to be found at higher flicker values (see Fig. 1). However, including such terms would make our relation no longer purely photometric, which we would argue is the principal benefit of the flicker technique.

Whilst we direct those interested to Kipping (2014) for details on the theory and range of effects which can cause AP discrepancies, we here provide an example calculation of the sensitivity of AP using flicker to detect eccentric exoplanets via the so-called “photo-eccentric” effect (Dawson & Johnson 2012). For a planet on an eccentric orbit, the derived light curve stellar density will differ from the true value by (Kipping 2010):

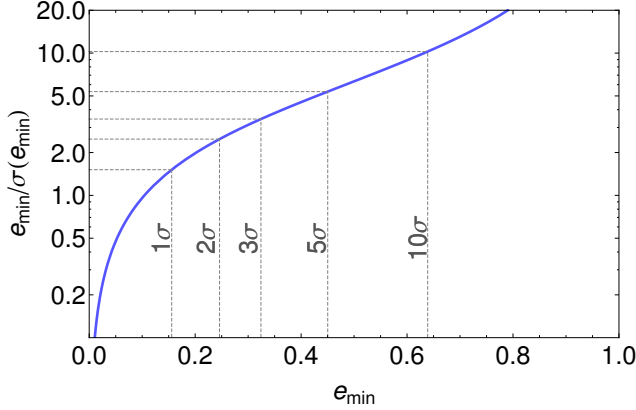


FIG. 3.— Sensitivity of flicker to detecting eccentric exoplanets via the photo-eccentric effect. We here assume a fractional error in $\rho_{\star, \text{true}}$ from a flicker-based measurement of 31.7%. Several key confidence levels are marked with dashed grid lines for reference.

$$\left(\frac{\rho_{\star, \text{obs}}}{\rho_{\star, \text{true}}} \right) = \frac{(1 + e \sin \omega)^3}{(1 - e^2)^{3/2}}, \quad (8)$$

where e is the orbital eccentricity and ω is argument of periastron. Dawson & Johnson (2012) show how to first order, constraints on e scale with $\rho_{\star, \text{true}}^{1/3}$ and thus even a weak prior on the density can lead to useful constraints on e . With one observable and two unknowns, a unique solution to Equation 8 is not possible. However, one can derive the minimum eccentricity, e_{min} , of the planet and the associated uncertainty, $\sigma_{e_{\text{min}}}$, using Equations 39&40 of Kipping (2014) respectively. Let us assume that the uncertainty in $(\rho_{\star, \text{obs}}/\rho_{\star, \text{true}})$ is dominated by the denominator's error, which in turn was found using our flicker relation and equals 31.7%. We may now plot the term $(e_{\text{min}}/\sigma_{e_{\text{min}}})$ as a function of e_{min} in Fig. 3, to illustrate the ability of flicker to detect eccentric planets. Using the classic Lucy & Sweeney (1971) test, we mark several key confidence levels with grid lines, demonstrating that flicker can detect eccentricities of $e_{\text{min}} = 0.25$ to $\geq 2\sigma$ confidence and $e_{\text{min}} = 0.32$ to $\geq 3\sigma$. With the power of large number statistics, we anticipate that flicker will be particularly powerful for inferring the ensemble distribution of orbital eccentricities.

4.2. Implications

Between the two catalogs of Huber et al. (2013) and Chaplin et al. (2014), there are 588 unique targets with asteroseismology detections yielding ρ_{\star} measurements with a median uncertainty of 4.1%. In contrast, there are 28,577 *Kepler* targets with $K_P < 14$, $4500 < T_{\text{eff}} < 6500$ K and $3.25 < \log g < 4.43$ (NASA Exoplanet Archive). Making the simple assumption that the same fraction of these targets will satisfy the range criterion defined earlier in §3.1, then we expect $\sim 25,000$ targets to be amenable for a flicker-based estimate of ρ_{\star} with a model accuracy of 31.7%. This translates to an increase in the number of AP targets by a factor of ~ 40 at the expense of an increase in the measurement uncertainty by a factor of ~ 8 . By any accounts, this is an acceptable compromise and opens the door to conducting AP on hundreds of *Kepler* planetary candidates (we estimate

~ 630).

An alternative method to determine $\rho_{\star, \text{true}}$ for targets without detectable oscillations would be via spectroscopy (e.g. Dawson & Johnson 2012). Here, one observes a spectrum of the target, compares it to a catalog of library spectra with various T_{eff} , $[M/H]$ and $\log g_{\star}$ and then finally one finds the best matching stellar evolution isochrones to these basic parameters. This procedure has several drawbacks compared to a flicker-based determination though. Firstly, this method requires that one obtain high SNR spectra, whereas F8 can be measured from the data obtained directly from a photometric mission like *Kepler*. Secondly, the final determination of ρ_{\star} is strongly model dependent using both stellar evolution models and spectra template matching laden with challenging degeneracies. Finally, it is worth noting that the formal uncertainty on a spectroscopic determination of $\rho_{\star, \text{true}}$ is typically no better than the flicker-based empirical relation for Sun-like stars. For example, Dawson & Johnson (2012) report $\rho_{\star, \text{true}} = 1.02^{+0.45}_{-0.29} \rho_{\odot}$ for the $K_P = 13.6$ Sun-like target KOI-686 and our flicker technique yields $(0.97 \pm 0.44) \rho_{\odot}$. In general then, we argue that for determinations of ρ_{\star} , the empirical and largely model independent flicker technique is preferable to spectroscopy, provided the target satisfies our sample criteria.

For the future TESS mission (Ricker et al. 2010), the smaller lens aperture of 12 cm will lead to higher photon noise than *Kepler*, for the same target. We therefore expect the 14th magnitude cut-off of our flicker calibration to drop to ~ 11.5 . The same effect will lead to only very bright stars having asteroseismology detections though, with preliminary estimates suggesting $\sim 5 \times 10^3$ asteroseismology targets out of $\sim 5 \times 10^5$ target stars. In contrast, we expect that $\sim 10^5$ TESS targets will be amenable to a flicker-based determination of their stellar densities (with the exact number depending upon the as yet unknown target list). Similarly, we expect flicker to have majorly benefit the upcoming PLATO 2.0 mission (Rauer et al. 2013) for both moderately bright targets near the edge of the field and faint targets in the center. Since AP is not only a method for characterizing exoplanets but also for vetting them (Sliski & Kipping 2014), then we expect flicker to be an invaluable tool in the TESS and PLATO era.

ACKNOWLEDGEMENTS

DMK is supported by the NASA Sagan Fellowships. FAB is supported by the NASA Harriet Jenkins Fellowship and a Vanderbilt Provost Graduate Fellowship. WJC acknowledges financial support from the UK Science and Technology Facilities Council. DH acknowledges support by an appointment to the NASA Postdoctoral Program at Ames Research Center, administered by Oak Ridge Associated Universities through a contract with NASA, and support by the Kepler Participating Scientist Program.

REFERENCES

- Akeson, R. L. et al., 2013, *PASP*, 125, 989
- Baglin, A., Michel, E., Auvergne, M. & COROT Team, 2006, in *Proc. of the CoRoT Mission Pre-Launch StatusStellar Seismology and Planet Finding*, ed. M. Fridlund, A. Baglin, J. Lochard & L. Conroy (ESA SP-1306; Noordwijk: ESA), 39
- Barnes, S. A., 2007, *ApJ*, 669, 1167
- Basri, G. et al., 2011, *AJ*, 141, 20
- Bastien, F. A., Stassun, K. G., Basri, G. & Pepper, J., 2013, *Nature*, 500, 427 (B13)
- Belkacem, K. et al., 2011, *A&A*, 530, 142
- Borucki, W. et al., 2008, in Pont F., Sasselov, D., Holman M. J., eds, *Proc. IAU Symp. 253: Transiting Planets*, p. 289
- Brown, T. M., Gilliland, R. L., Noyes, R. W. & Ramsey, L. W., 1991, *ApJ*, 368, 599
- Bruntt, H. et al., 2012, *MNRAS*, 423, 122
- Chaplin, W. J., Houdek, G., Appourchaux, T., Elsworth, Y., New, R. & Toutain, T., 2008, *A&A*, 485, 813
- Chaplin, W. J. & Miglio, A., 2013, *ARA&A*, 51, 353
- Chaplin, W. J. et al., 2014, *ApJS*, 210, 1
- Cranmer, S. R., Bastien, F. A., Stassun, K. G. & Saar, S. H., 2014, *ApJ*, 781, 124
- Dawson, R. I. & Johnson, J. A., 2012, *ApJ*, 756, 13
- Deming, W. E., 1943, *Statistical Adjustment of Data*, Wiley, New York, NY
- Epstein, C. R. & Pinsonneault, M. H., 2014, *ApJ*, 780, 159
- Huber, D. et al., 2013, *ApJ*, 767, 127
- Kipping, D. M., 2010, *MNRAS*, 407, 301
- Kipping, D. M., Dunn, W. R., Jasinski, J. M. & Manthri, V. M., 2012, *MNRAS*, 421, 1166
- Kipping, D. M., 2013, *MNRAS*, 434, L51
- Kipping, D. M., 2014, *MNRAS*, accepted (astro-ph:1311.1170)
- Kjeldsen, H. & Bedding, T. R., 1995, *A&A*, 293, 87
- Lucy, L. B. & Sweeney, M. A., 1971, *AJ*, 76, 544
- Mathur, S. et al., 2011, *ApJ*, 741, 119
- Rauer, H et al., 2013, *Exp. Astron.*, submitted (astro-ph:1310.0696)
- Ricker, G. R. et al., 2010, in *American astronomical society meeting abstracts #215*, vol. 42 of *Bulletin of the American Astronomical Society*, p. 450.06
- Seager, S. & Mallen-Ornelas, G., 2003, *ApJ*, 585, 1083
- Skumanich, A., 1972, *ApJ*, 171, 565
- Sliski, D. H. & Kipping, D. M., 2014, *ApJ*, submitted (astro-ph:1401.1207)
- Ulrich, R. K., 1986, *ApJ*, 306, L37
- Walkowicz, L. M. & Basri, G. S., 2013, *MNRAS*, 436, 1883
- White, T. R., Bedding, T. R., Stello, D., Christensen-Dalsgaard, J., Huber, D. & Kjeldsen, H., 2011, *ApJ*, 743, 161
- Wright, J. T., 2005, *PASP*, 117, 657